Korean J. Chem. Eng., **29**(9), 1151-1157 (2012)
DOI: 10.1007/s11814-012-0038-8

CO oxidation over CuO catalysts prepared with different precipitants

Jung-Hyun Park*, Jun Hee Cho*, Kyung Ho Cho, Tae Woo Lee***, Hyun Sik Han***, and Chae-Ho Shin*,†**

*Department of Chemical Engineering, Chungbuk National University, Cheongju, Chungbuk 361-763, Korea
**Green Chemistry Division, Korea Research Institute of Chemical Technology, Yuseong, Daejeon 305-600, Korea
***R&D Center, Heesung Catalysts Corp., #507-1Da, Jungwang-dong, Shiheung-city, Gyeonggi-do 429-450, Korea
(*Received 13 February 2012 • accepted 14 March 2012*)

Abstract−CuO catalysts, prepared by the precipitation method using different precipitants such as ammonium hydroxide, sodium hydroxide, sodium carbonate and sodium hydrogen carbonate were applied to CO oxidation. Among the catalysts studied, CuO synthesized with sodium hydrogen carbonate showed the highest activity for CO oxidation. With the water vapor present in the feed gas, the catalytic activity decreased considerably due to reduction in the number of active sites by competitive adsorption between water vapor and CO. The H_2-TPR and CO-TPD results showed that existing Na^+ cations and HCO_3^- and CO_3^{2-} anions on the CuO surface could weaken the copper-oxygen bond strength and accelerate the mobility of oxygen on the surface or lattice. Finally, the morphology of the CuO crystals was dependent on the precipitants, and the introduction of Na^+ cations and various anions resulted in the formation of smaller crystals.

Key words: CuO Catalyst, Precipitants, CO Oxidation, H_2-TPR, CO-TPD

INTRODUCTION

The catalytic oxidation of carbon monoxide is an important process in the three-way catalytic treatment of the exhaust gas from automobiles and in the selective oxidation of CO in reformer gas for fuel cell applications. Precious metals such as Pt, Pd, Au and Rh have good activity and stability for the oxidation of CO [1]. But despite their good activity, precious metals have limitations as catalysts due to their high costs. Recently, considerable research has focused on base metal catalysts for CO oxidation. Transition metals as Cu, Co, and Ni have been recognized as useful CO oxidation catalysts. In particular, copper-based catalysts have shown good catalytic activity and selectivity for CO oxidation in hydrogen-rich streams (PROX reaction) [2]. In addition, copper oxide supported on ceria has shown good activity in low temperature CO oxidation [3]. The Cu-Mn-O-system is a well-known oxidation catalyst for CO oxidation at room temperature. Spinel-type $CuMn_2O_4$, known as hopcalite, is commercially employed to remove CO and NO_x air pollutants from exhaust gas [4]. For CO oxidation, the high activity of the Cu-Mn-O-system could be attributed to the resonance system $Cu^{2+}Mn^{+}/Cu^{+}Mn^{4+}$ and the preferential adsorption of CO on Cu^{2+}/Mn^{3+} and O_2 on Cu^{+}/Mn^{3+}, respectively [5].

Generally, CO oxidation catalytic performance is strongly influenced by the precipitants and methods used in catalyst preparation. In particular, alkali metals such as Li, Na, K, Cs, and Rb are frequently used as effective promoters. The CuO-CeO_2 mixed oxide catalyst prepared by co-precipitation with different ratios of KOH/K_2CO_3 exhibited high catalytic activity, which was a result of the combined effect of CuO and CeO_2 for CO oxidation and the residual K^+ for the preferential oxidation of CO in excess hydrogen (PROX) [6]. Tanaka et al. [7] reported that Pt/Al_2O_3 modified with potassium was effective in the PROX reaction. Furthermore, the effect of alkali metals (Li, Na, K, Rb, Cs) on the PROX reaction over Pt catalysts supported on Al_2O_3 has been investigated [8]. For preferential CO oxidation in H_2-rich gas streams, the effect of added alkali metal ions over Pt/Al_2O_3 was greatly dependent on the additive amount. The order of the promoting effect was K>Na>Rb>Cs, which can be related to a moderate strength of the basicity of the alkali metal. Mirkelamoglu et al. [9] found that Na^+ promoted PdO/SnO_2 enhanced the CO oxidation rate and decreased the light-off temperature. The alkali metal-promoted catalyst was also used for the catalytic decomposition of NO and N_2O [10,11].

The purpose of the present study was to investigate the influence of coexisting Na^+ cations and anions of OH^-, HCO_3^- and CO_3^{2-} on CuO catalysts, which showed good catalytic performance in CO oxidation. We prepared CuO catalysts using different precipitants such as ammonium hydroxide (AH), sodium hydroxide (SH), sodium carbonate (SC) and sodium hydrogen carbonate (SHC), and evaluated their performance in CO oxidation. The prepared catalysts were characterized by X-ray diffraction (XRD), N_2 sorption, inductively coupled plasma and atomic emission spectrometry (ICP-AES), temperature-programmed reduction of H_2 (H_2-TPR) and temperature-programmed desorption of CO (CO-TPD). The information derived from these characterization techniques was correlated with the CO oxidation activity.

EXPERIMENTAL

1. Preparation of Catalysts

The catalysts were prepared by a conventional precipitation method with different precipitants, such as ammonium hydroxide (AH, NH_4OH, Samchon, 25-28 vol%), sodium hydroxide (SH, NaOH, Junsei, 96%), sodium carbonate (SC, Na_2CO_3, Wako, 99%), and sodium

†To whom correspondence should be addressed.
E-mail: chshin@chungbuk.ac.kr

hydrogen carbonate (SHC, $NaHCO_3$, Hayashi, 99.5%). Each aqueous solution of AH, SH, SC, or SHC was controlled to 1 M and the precipitant solution was added to 200 mL copper nitrate ($Cu(NO_3)_2 \cdot 2.5\ H_2O$, Junsei, 98%) solution until the pH reached 7. The resulting solution was aged at room temperature for 12 h and then filtered. The filtered precipitate was washed with 1 L de-ionized water. The washed cake was dried at 100 °C for 12 h and then calcined in flowing air at 300 °C for 2 h. The calcined catalysts were denoted CuO-AH, CuO-SH, CuO-SC and CuO-SHC.

The influence of changing quantities of residual Na^+ cation and surface carbonate species on the catalyst surface could be investigated by varying the number of filter cake washes. CuO-SHC catalysts were prepared in the manner described above, and the filtered catalysts were washed 1, 3, or 5 times with 1 L de-ionized water. The catalysts were denoted CuO-SHC-x, in which x represents the number of washings.

2. Catalyst Characterization

Powder X-ray diffraction (XRD) patterns were collected on a Siemens D5005 diffractometer with Cu Kα radiation (λ=0.15468 nm) at 30 kV and 50 mA. The crystalline particle size was calculated from the (-111) line of the CuO crystal using the Scherrer equation. The Brunauer-Emmett-Teller (BET) surface area and total pore volume were measured by N_2 adsorption using a Micromeritics ASAP 2020. Prior to measurement, the samples were degassed for 4 h under vacuum at 250 °C. The BET surface area was determined by the BET in the range of P/P_o=0.05-0.20 and the total pore volume was measured at P/P_o=0.99. The alkali metal content of the catalysts was obtained with a Jarrell-Ash Polyscan 61E inductively coupled plasma and atomic emission spectrometer (ICP-AES). Scanning electron microscopy (SEM) images of the catalysts were acquired on a Hitachi S-2500C scanning electron microscope at an acceleration voltage of 5 kV. The IR spectra were recorded on a FT-IR spectrophotometer (Bruker Optic IFS 66/S).

Temperature-programmed reduction of H_2 (H_2-TPR) was performed in a fixed-bed quartz reactor with the effluent gases monitored by quadruple mass spectroscopy (QMS, Pfeiffer Vacuum QMS 200). Prior to the H_2-TPR experiment, a 0.05 g sample was loaded in a quartz reactor (I. D. 12 mm) and pretreated at 300 °C in a He flow for 1 h. After cooling to RT, a flow of 5% H_2/Ar was passed through the sample and the temperature was raised from RT to 600 °C at a rate of 10 °C min^{-1}. The mass signal of H_2 (m/z=2) was detected by QMS.

CO-temperature programmed desorption (CO-TPD) was performed in a fixed-bed reactor with the effluent gases monitored by QMS. Prior to the CO-TPD experiment, 0.1 g sample was treated with He (50 $cm^3 \cdot min^{-1}$) at 300 °C for 1 h, then cooled to RT in the same atmosphere. After that, the sample was adsorbed with 5% CO/N_2 (50 $cm^3 \cdot min^{-1}$) for 1 h and subsequently flushed by He (50 $cm^3 \cdot min^{-1}$) for 0.5 h to remove physisorbed CO molecules. Finally, the temperature was increased to 700 °C at a heating rate of 10 °C·min^{-1} under flowing He (50 $cm^3 \cdot min^{-1}$). The mass signals of CO (*m/z*=28) and CO_2 (*m/z*=44) produced during the experiment were recorded. Furthermore, to investigate the effect of water vapor on CO oxidation, CO-TPD was performed after two different treatments. After pretreatment, two kinds of adsorption were carried out: (1) CO adsorption (3 kPa) at 30 °C for 1 h and (2) CO (3 kPa)+H_2O (3 kPa) co-adsorption at 30 °C for 1 h. After adsorption, the catalyst sample was flushed in flowing He (50 $cm^3 \cdot min^{-1}$) at 30 °C for 0.5 h and then heated from 30 to 700 °C at 10 °C min^{-1}.

X-ray photoelectron spectroscopic (XPS) measurements were performed on a VG Scientific ESCALAB 210 spectrometer with a Mg Kα X-ray source (1,253.6 eV). Each sample was degassed at 1×10^{-6} Torr for 4 h to remove volatile contaminants, and the pressure inside the analysis chamber was maintained under 5×10^{-10} Torr. All the binding energies were referenced to the C 1s peak at 284.6 eV from adventitious carbon. The binding energy values reported here were within an accuracy of ±0.3 eV.

3. Catalytic Performance for CO Oxidation

The catalytic oxidation of carbon monoxide was carried out at atmospheric pressure in a continuous-flow microreactor. Prior to the catalytic reaction, 0.1 g catalyst was activated under flowing He (150 $cm^3 \cdot min^{-1}$) at 300 °C for 1 h. The composition of the dry feed gases was 1 vol% CO, 20 vol% O_2 and 79 vol% N_2 with a total flow rate of 150 $cm^3 \cdot min^{-1}$ and it was heated at a rate of 2 °C·min^{-1} from 50 to 250 °C. In addition, the effect of water vapor was examined by introducing a continuous flow, of 3% H_2O vapor through a saturator. The conversion of CO was calculated in terms of the CO mole balance. The concentration of CO in the effluent stream was measured every second using an on-line CO analyzer (Teledyne Instrument Analyzer of IR-ways).

RESULTS AND DISCUSSION

Powder XRD patterns of the CuO catalysts prepared with different precipitants are shown in Fig. 1. All solid peaks typically represent the crystalline structure of cubic CuO [12]. The XRD peaks of CuO prepared by using alkali-precipitants containing Na^+ were broadened compared to those of CuO-AH. The average crystallite sizes of the CuO catalysts estimated by the CuO (111) plane are reported in Table 1. The crystallite sizes of CuO-AH, CuO-SH, CuO-SC, and CuO-SHC were 12.8, 11.0, 6.9, and 6.4 nm, respectively. The existing Na^+ cation and HCO_3^- and CO_3^{2-} anions of the CuO catalysts promoted the formation of smaller crystallite sizes. However, the absence of peak position changes meant that substitution of the

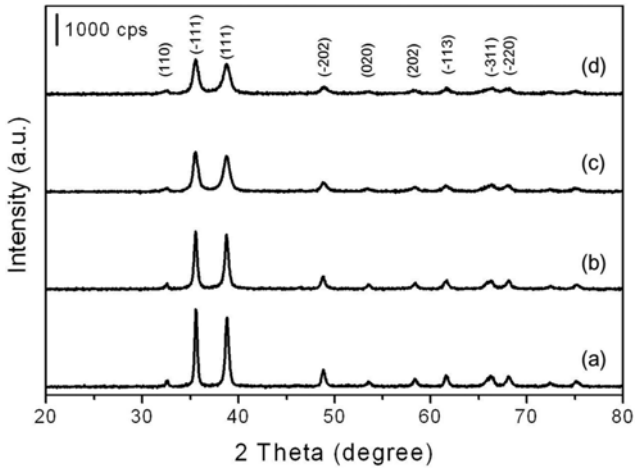

Fig. 1. XRD patterns of CuO catalysts prepared with different precipitants: (a) CuO-AH, (b) CuO-SH, (c) CuO-SC, and (d) CuO-SHC.

Table 1. Physical properties of the CuO-x catalysts

Catalyst[a]	S_{BET} ($m^2\ g^{-1}$)	Pore volume ($cm^3\ g^{-1}$)	Crystallite size (nm)[c]	Na (wt%)[d]
CuO-AH	5.9	0.03	12.8	-
CuO-SH	16.8	0.03	11.0	0.010
CuO-SC	38.7	0.39	6.9	0.105
CuO-SHC (CuO-SHC-1[b])	40.2	0.29	6.4	0.130
CuO-SHC-3	33.4	0.28	6.9	0.078
CuO-SHC-5	33.0	0.23	7.1	0.011

[a]Precipitants used to control pH for the synthesis of CuO; AH (ammonium hydroxide), SH (sodium hydroxide), SC (sodium carbonate), and SHC (sodium hydrogen carbonate)
[b]Number of washes
[c]Determined by Scherrer's equation
[d]Analyzed by elemental analysis

Na^+ cation into the Cu^{2+} position of Cu-O was not facile (ionic radii, r_{Na+}=1.16 Å, r_{Cu2+}=0.87 Å and r_{Cu1+}=0.91 Å) [13]. If the Cu^{2+} ions in the CuO lattice had been replaced by Na^+ ions, the lattice parameters of CuO would have been altered. This implies that Na^+ ions were not incorporated in the CuO lattice.

The BET surface area, total pore volume and elemental analyses of residual Na^+ in the CuO catalysts are given in Table 1. The nitrogen adsorption isotherm exhibited a distinct hysteresis at P/P_o= 0.65-0.80 due to the presence of 20-30 nm mesopores. The precipitants influenced the surface area and pore volume. When residual Na^+ species increased from 0.010 wt% (CuO-SH) to 0.130 wt% (CuO-SHC), the surface area markedly increased from 16.8 to 40.2 $m^2\ g^{-1}$.

Fig. 2 shows SEM images of CuO prepared with different precipitants. The morphologies and particle sizes of the CuO catalysts greatly depended on the precipitants added to synthesis mixtures. CuO-AH exhibited thin plate crystal shapes, whereas CuO-SH was a mixture of rod and plate types, and CuO-SC and CuO-SHC were almost all small rod-type crystals. The introduction of alkali precipitants resulted in smaller crystals than those from AH; in particular, the addition of carbonate species in the synthesis mixture led to smaller crystals. This may be due to the prevention of Cu nanoparticles agglomeration, which results in increased surface area and pore volume.

XPS analysis was performed to elucidate the oxidation states of

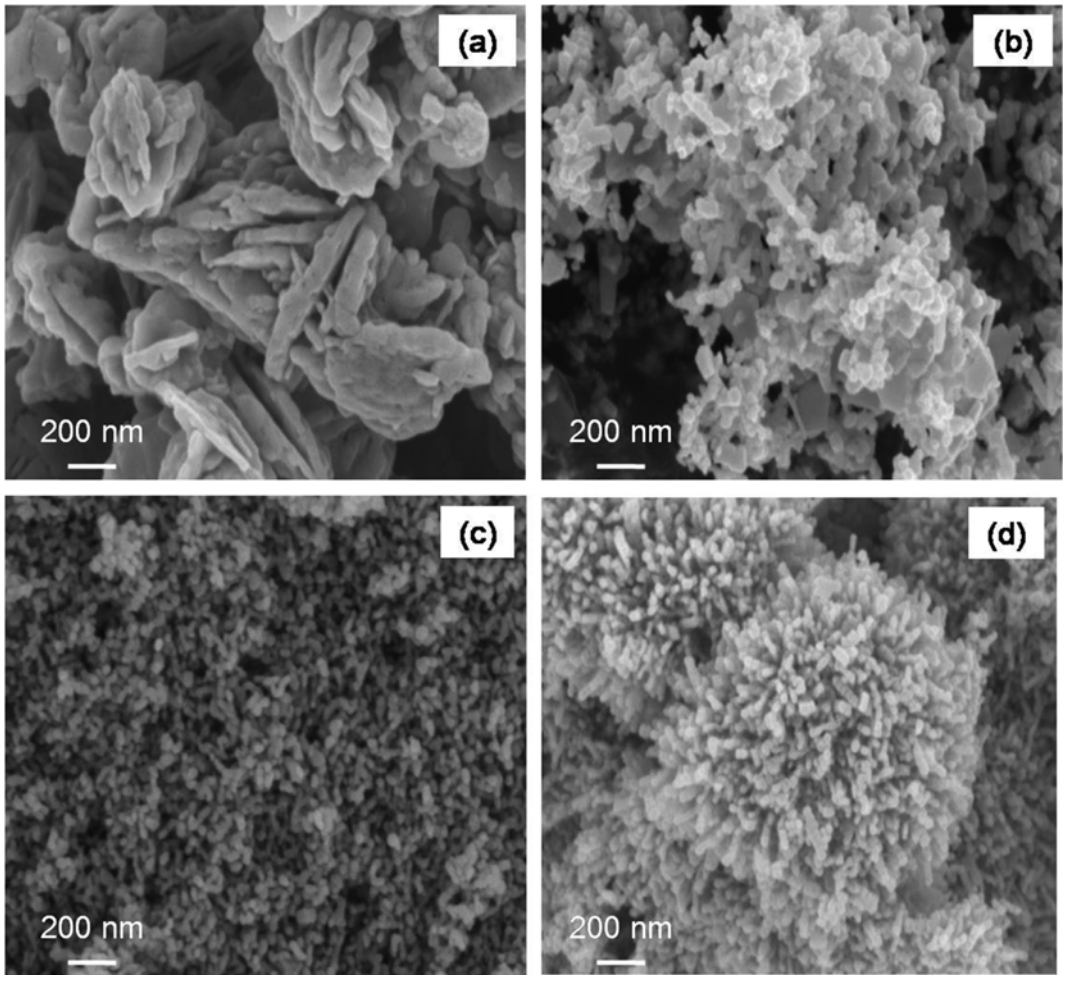

Fig. 2. SEM images of CuO catalysts prepared with different precipitants: (a) CuO-AH, (b) CuO-SH, (c) CuO-SC, and (d) CuO-SHC calcined at 300 °C for 2 h.

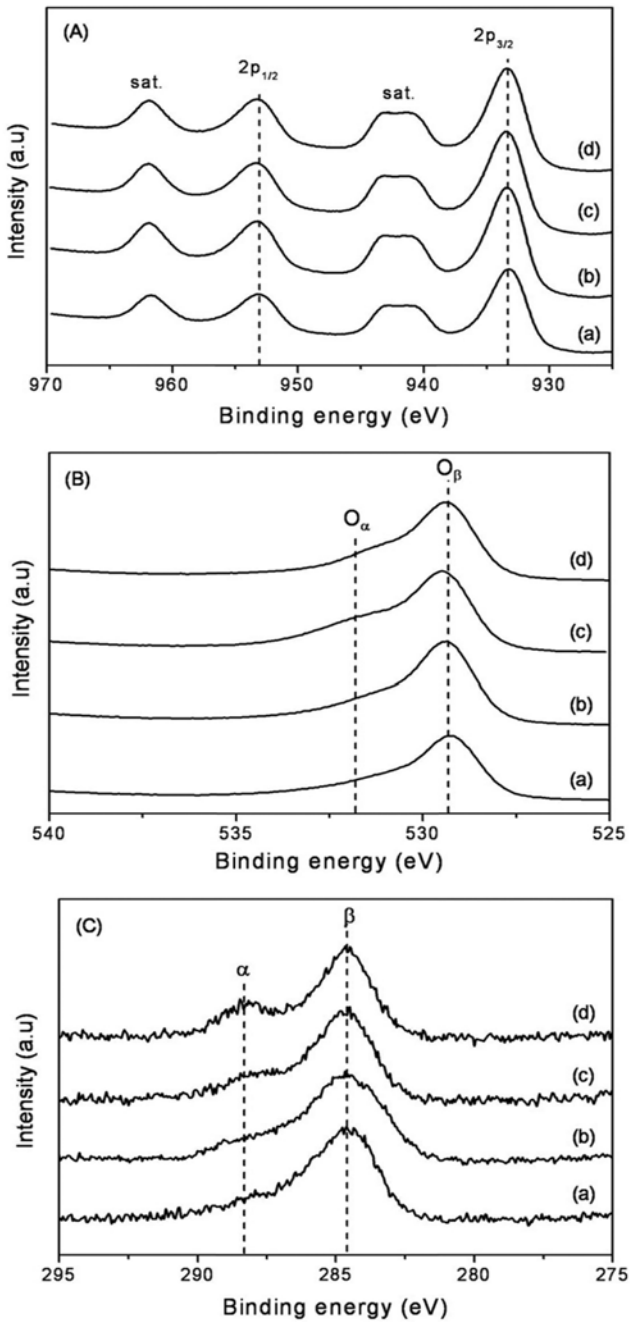

Fig. 3. XPS spectra of (A) Cu 2p, (B) O 1s, and (C) C 1s of the CuO-x catalysts: (a) CuO-AH, (b) CuO-SH, (c) CuO-SC, and (d) CuO-SHC.

copper and oxygen in CuO; the results are shown in Fig. 3. All the catalysts had a similar binding energy at 933.6 eV for $Cu_{2p3/2}$. It is well known that electron donation from alkali cation to transition metals takes place at the interface, resulting in a decrease of the work function and then a translation of the whole system towards a lower binding energy [11,14,15]. The reduction of binding energy values indicates a change in the electronic state of copper upon the addition of alkali cations. The insignificant change in the binding energy of our catalyst system may be ascribed to the presence of residual alkali cations on the CuO surface in amounts insufficient to change the electronic state of copper. As shown in Fig. 3(B), the O 1s peaks

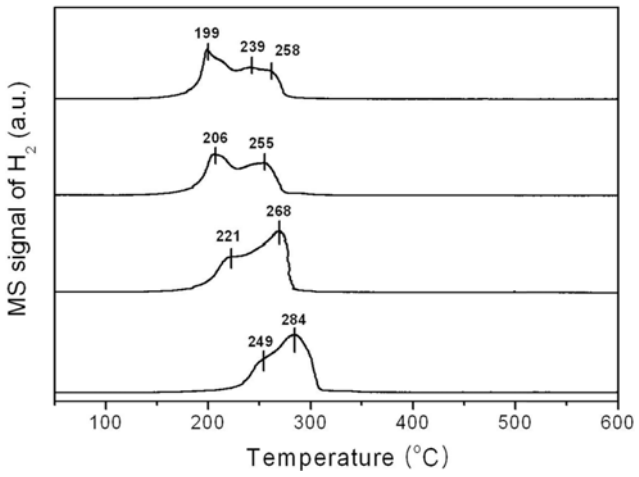

Fig. 4. H_2-TPR profiles of CuO-x catalysts: (a) CuO-AH, (b) CuO-SH, (c) CuO-SC, and (d) CuO-SHC. Conditions: 5% H_2/Ar=50 cm^3 min^{-1}, heating rate=10 °C min^{-1}, catalyst weight =0.05 g.

consisted of one main peak and a shoulder that were from lattice oxygen (O^{2-}) at 529.6-530.0 eV and surface-adsorbed oxygen as O_2^{2-} or O^-, OH^-, and CO_3^{2-} at 531.3-531.7 eV, respectively [16]. XPS spectra of C 1s are shown in Fig. 3(C). The peaks at 285 eV (denoted β), and 288 eV (denoted α) correspond to adventitious carbon and surface carbonate species, respectively. The C 1s peak intensity at 288 eV for CuO-x prepared using precipitants containing carbonate anions was stronger than those for AH and SH. This indicates the strong adsorption of carbonate anions on the CuO catalysts.

The H_2-TPR profiles for CuO catalysts prepared with different precipitants are shown in Fig. 4. All the catalysts exhibited complex reduction peaks, indicating the existence of two or three different copper oxide species. The TPR peak temperatures of CuO catalysts containing Na^+ cations were lower than that of CuO-AH. In case of CuO catalysts containing Na^+, the intensity of the low-temperature peak increased with Na^+ loading. CuO-AH showed two reduction peaks at 249, and 284 °C, and CuO-SHC showed three reduction peaks in minimum at 199, 239 and 258 °C. According to the literature [17-21], the low-temperature peak can be ascribed to the reduction of Cu^{2+} to Cu^{1+} or finely dispersed nano-size copper oxide species, while the higher one is due to the reduction of Cu^{1+} to Cu^0 or bulk copper oxide species, including large clusters. Therefore, the copper reduction peaks may be assigned to the reduction of finely dispersed CuO species, isolated Cu^{2+} ions, and larger particles of bulk CuO.

Several kinetic and mechanistic studies have been performed for the catalytic oxidation of CO [22,23]. The Mars-van Krevelen (MvK) mechanism has been widely accepted for CO oxidation. In the MvK mechanism, adsorbed CO reacts with labile lattice oxygen as noted in the following equation: CO (ads)+O^{2-} (lattice)+Cu^{2+}→CO_2 (ads) +Cu^{1+}. The reactivity is associated with the Cu oxidation state, Cu^{2+}/Cu^{1+} and the "oxygen mobility" in the oxide lattice. To determine the influence of residual alkali metals in the CuO catalyst on the basis of the MvK mechanism, CO-TPD was carried out (Fig. 5(A)). CO_2 (m/z=44) was mainly detected from the reaction between the adsorbed CO and lattice oxygen of the CuO catalysts, and a minor

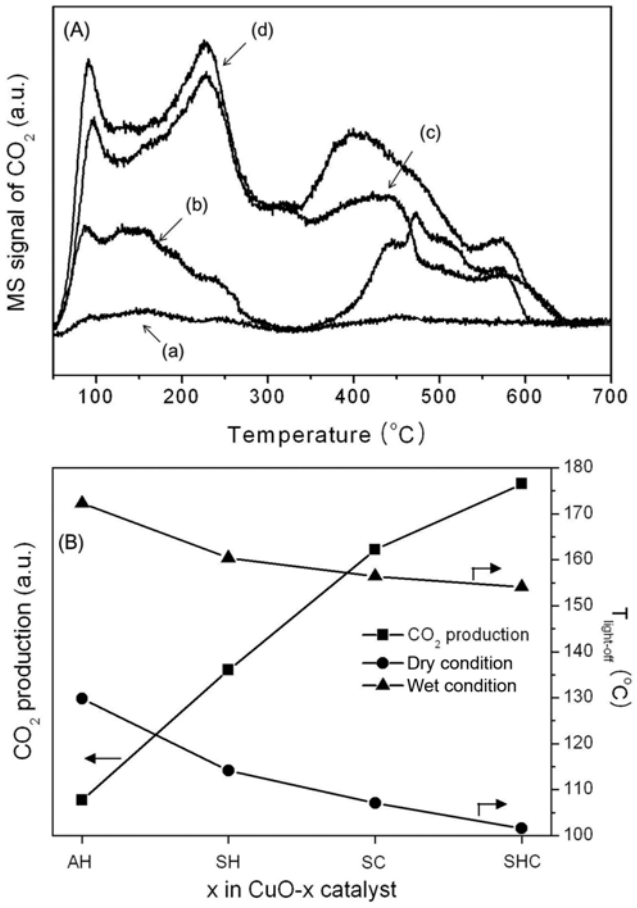

Fig. 5. (A) CO_2 production during the CO-TPD over CuO-x catalyst and (B) correlation between CO_2 production and catalytic activity: (a) CuO-AH, (b) CuO-SH, (c) CuO-SC, and (d) CuO-SHC.

amount of CO (*m/z*=28). The desorption patterns were very complex, meaning that CO adsorption sites existed in diverse forms. The quantitative amount of CO_2 desorbed could be correlated with CO oxidation activity. Four desorption peaks were primarily observed at 98, 230, 410 and 572 °C, suggesting four kinds from lattice oxygen of different environments. In the case of CuO-AH, a small, broad CO_2 desorption peak was observed in the 50-300 °C temperature range. However, the other catalysts, with residual Na^+ cations, led to lower light-off temperatures for CO oxidation. Fig. 5(B) shows the correlation between CO_2 production during the CO-TPD and the light-off temperature of the CuO-x catalysts. The quantity of CO_2 was calculated by integrating the CO-TPD profiles in the range of 50-300 °C. The CuO-SHC catalyst showed the largest CO_2 desorption peaks, i.e., the largest oxygen capacity. The order of the light-off temperature was CuO-AH>CuO-SH>CuO-SC>CuO-SHC. On the other hand, CO_2 production increased in the order CuO-AH< CuO-SH<CuO-SC<CuO-SHC. Among the catalysts tested, the CuO-SHC catalyst showed the best catalytic performance. Therefore, the oxygen capacity of CuO-x catalysts was influenced by the precipitant and was a crucial factor for determining catalytic performance in the oxidation of CO [24,25].

CO conversion as a function of reaction temperature in dry or wet conditions over CuO catalysts prepared with different precipitants is shown in Fig. SI 1. For the comparison of catalytic activity of $CuMn_2O_4$ catalyst prepared with Cu/Mn molar ratio of 1/2, the result is also shown in Table 2. The spinel type of $CuMn_2O_4$ catalyst showed low catalytic activity compared to that of CuO catalysts. The CuO-SHC catalyst showed the highest catalytic performance among the catalysts studied, exhibiting the lowest light-off temperature at 102 °C (Table 2). The catalytic activities of CuO catalysts containing small amounts of alkali cation were better than that of CuO-AH. In particular, as the residual Na^+ cation increased, the light-off temperature shifted considerably to lower temperature from 114 to 102 °C. A similar trend was also observed in the presence of 3% water vapor in the reactants. The light-off temperature of the CuO-SHC catalyst in wet conditions was 154 °C, shifted to a temperature of ~50 °C higher than in dry conditions. Under wet reaction conditions, the poor activity of CuO catalysts could be explained by the competitive adsorption of H_2O and CO molecules on the active sites [5,26].

To probe the poor catalytic activity in the presence of water vapor, CO-TPD was carried out. The CO-TPD profiles of the CuO-SHC catalyst after only CO adsorption and CO+H_2O co-adsorption are shown in Fig. 6. Regardless of the treatment conditions, the CO-

Table 2. CO catalytic activity of CuO-x catalysts prepared with different precipitants

Catalyst	Dry conditions[a]			Wet conditions[b]		
	$T_{20\%}$ (°C)	$T_{light-off}$ (°C)[c]	$T_{90\%}$ (°C)	$T_{20\%}$ (°C)	$T_{light-off}$ (°C)[c]	$T_{90\%}$ (°C)
CuO-AH	116.3	133.8	149.5	157.6	177.3	198.0
CuO-SH	99.2	114.1	126.8	142.2	160.4	179.1
CuO-SC	70.9	107.1	121.6	138.7	156.4	174.6
CuO-SHC (CuO-SHC-1[d])	57.5	101.6	118.3	137.2	154.1	172.6
CuO-SHC-3	95.7	112.6	128.8	139.4	157.3	177.7
CuO-SHC-5	103.4	122.1	140.4	143.6	162.2	183.7
$CuMn_2O_4$[e]	118.9	150.5	191.0	-	-	-

[a]$CO/O_2/N_2$=1/20/79 (mol ratio), GHSV=90,000 $cm^3 \cdot g_{cat.}^{-1} \cdot h^{-1}$, catalyst weight=0.1 g

[b]3% H_2O vapor was continuously supplied

[c]$T_{20\%}$, $T_{light-off}$ and $T_{90\%}$ refer to the temperature at 20, 50, and 90% conversion of CO, respectively

[d]Number of washing

[e]The catalyst was synthesized with Cu/Mn molar ratio of 1/2

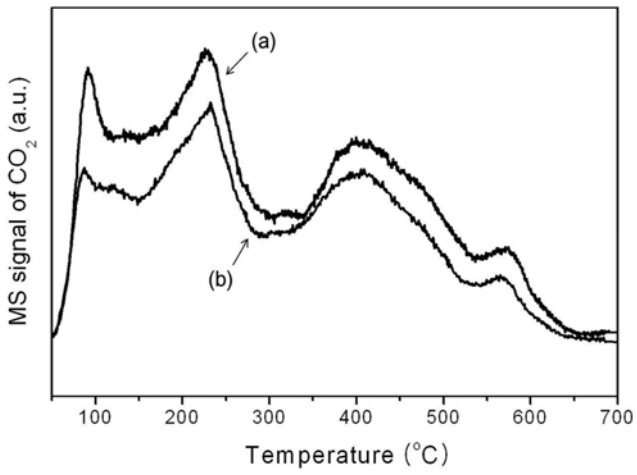

Fig. 6. CO_2 production during the CO-TPD over CuO-SHC catalyst after (a) only CO adsorption and (b) co-adsorption of $CO+H_2O$.

TPD patterns were almost identical. However, the amount of CO_2 desorption after only CO adsorption was larger than that after CO and H_2O co-adsorption. The amount of CO_2 desorption was calculated by integrating the curve of the CO_2 desorption peak, which reflects the total amount of lattice oxygen consumed for the reaction. The ratio of adsorption sites was found to be CO adsorption: $CO+H_2O$ co-adsorption=1 : 0.84. This result indicates that the supplied H_2O and CO molecules competitively adsorb on the active sites of the catalyst. Therefore, the large difference of $T_{light\text{-}off}$ could be attributed to competitive adsorption of CO and H_2O molecules on the same active sites for CO oxidation.

To elucidate the influence of the residual Na^+ cation and surface carbonate species on the catalyst surface, the CuO-SHC catalyst, which had shown the best catalytic activity, was prepared several more times; however, the number of washes was varied to diminish the quantity of residual Na^+ cation. The BET surface area, total pore volume and Na^+ content of the CuO-SHC-x catalyst decreased slightly with increased numbers of washes (Table 1). The catalytic activity of CuO-SHC-x catalysts in dry conditions decreased with increased numbers of washes (resulting in decreased residual Na^+ cations), and the light-off temperature of CuO-SHC-1and CuO-SHC-5 catalysts increased from 102 to 122 °C (Table 2 and SI 3). A similar trend was observed under wet reaction conditions. IR analysis was used to investigate the types and amount of carbonate species on the CuO-SHC-x catalysts obtained with the various of washing conditions. As shown in Fig. 7, two bands at 1,354 and 1,481 cm^{-1} were assigned to the adsorption of surface carbonates [27], and their intensities were nearly stable and independent of the number of washes. Therefore, the surface carbonate species of the CuO-SHC-x catalyst might not influence its activity toward CO oxidation [28].

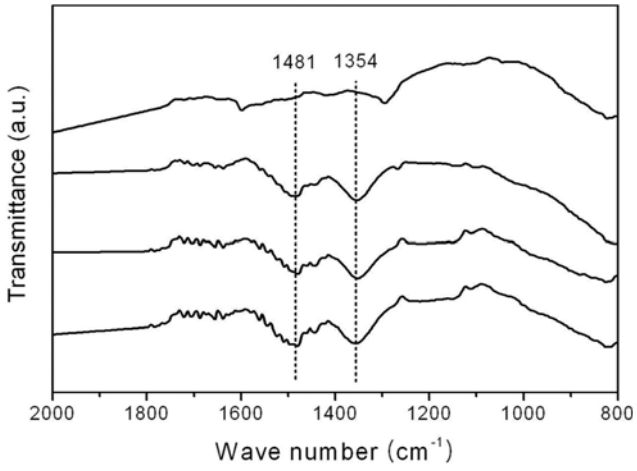

Fig. 7. FT-IR spectra of CuO-SHC-x catalysts prepared with different numbers of washes; (a) CuO-AH, (b) x=1 in CuO-SHC-x, (c) 3, and (d) 5, where x represents that the number of washing.

The stability of CuO catalysts was examined over CuO-AH and CuO-SHC catalysts (Fig. SI 2). The total conversion of CO over CuO-SHC catalyst was constantly maintained for 5 h without deactivation; however, the catalytic activity of CuO-AH catalyst slowly decreased.

CONCLUSIONS

CuO catalysts prepared using different precipitants were applied to CO oxidation. The morphology, crystallinity, and catalytic activity of the CuO-x catalysts were dependent on the nature of the precipitants added to the synthesis mixture. Among the catalysts studied, CuO-SHC catalyst prepared with sodium hydrogen carbonate showed the best activity under dry and wet reaction conditions. The oxygen capacity of the CuO-x catalyst was influenced by the precipitants used; the quantity of residual Na^+ ions was a crucial factor in determining the catalytic performance in CO oxidation. From the combined CO-TPD and H_2-TPR results, the residual Na^+ cations on the CuO catalyst led to weakened metal-oxygen interactions and accelerated the mobility of oxygen on the surface or lattice, resulting in an enhancement of the catalytic activity for CO oxidation.

ACKNOWLEDGEMENT

This work was financially supported by a grant from the Industrial Source Technology Development Programs (2009-10033479) of the Ministry of Knowledge Economy (MKE) of Korea.

SUPPORTING INFORMATION

Additional information as noted in the text. This information is available via the Internet at http://www.springer.com/chemistry/journal/11814.

REFERENCES

1. S. Royer and D. Duprez, *Chem. Cat. Chem.*, **3**, 24 (2011).
2. T. Valdés-Solís, I. López and G. Marbán, *Int. J. Hydrog. Energy*, **35**, 1879 (2010).
3. M. Luo, Y. Zhong, X. Yuan and X. Zheng, *Appl. Catal. A: Gen.*, **162**, 121 (1997).
4. G. Fortunato, H. R. Oswald and A. Reller, *J. Mater. Chem.*, **11**, 905 (2001).

5. S. Vepřek, D. L. Cocke, S. Kehl and H. R. Oswald, *J. Catal.*, **100**, 250 (1986).
6. P. Zhu, J. Li, S. Zuo and R. Zhou, *Appl. Surf. Sci.*, **255**, 2903 (2008).
7. H. Tanaka, M. Kuriyama, Y. Ishida, S. Ito, T. Kubota, T. Miyao, S. Naito, K. Tomishige and K. Kunimori, *Appl. Catal. A: Gen.*, **343**, 125 (2008).
8. Y. Minemura, M. Kuriyama, S. Ito, K. Tomishige and K. Kunimori, *Catal. Commun.*, **7**, 623 (2006).
9. B. Mirkelamoglu and G. Karakas, *Appl. Catal. A: Gen.*, **299**, 84 (2006).
10. L. Xue, C. Zhang, H. He and Y. Teraoka, *Catal. Today*, **126**, 449 (2007).
11. N. Pasha, N. Lingaiah, P. Reddy and P. Prasad, *Catal. Lett.*, **127**, 101 (2009).
12. C. Zhang, Y. Bai, Y. Yin, J. Gu and Y. Sun, *Korean J. Chem. Eng.*, **28**, 602 (2011).
13. http://en.wikipedia.org/wiki/Ionic_radius.
14. R. Fernández, J. Estelle, Y. Cesteros, P. Salagre, F. Medina, J. Sueiras and J. G. Fierro, *J. Mol. Catal. A: Chem.*, **119**, 77 (1997).
15. C. Ohnishi, K. Asano, S. Iwamoto, K. Chikama and M. Inoue, *Catal. Today*, **120**, 145 (2007).
16. J. P. Holgado, G. Munuera, J. P. Espinós and A. R González-Elipe, *Appl. Surf. Sci.*, **158**, 164 (2000).
17. W. J. Park, H. J. Jeong, W. L. Yoon, C. S. Kim, D. K. Lee, Y. K. Park and Y. W. Rhee, *Int. J. Hydrog. Energy*, **30**, 209 (2005).
18. G. Avgouropoulos, T. Ioannides and H. Matralis, *Appl. Catal.: B Environ.*, **56**, 87 (2005).
19. M. Luo, J. Ma, J. Lu, Y. Song and Y. Wang, *J. Catal.*, **246**, 52 (2007).
20. W. Dow, Y. Wang and T. Huang, *J. Catal.*, **160**, 155 (1996).
21. Z. Wu, H. Zhu, Z. Qin, H. Wang, J. Ding, L. Huang and J. Wang, *Fuel*, http://dx.doi.org/10.1016/j.fuel.2010.03.001.
22. K. Ramesh, L. Chen, F. Chen, Y. Liu, Z. Wang and Y. Han, *Catal. Today*, **131**, 477 (2008).
23. K. Morgan, K. J. Cole, A. Goguet, C. Hardacre, G. J. Hutchings, N. Maguire, S. O. Shekhtman and S. H. Taylor, *J. Catal.*, **276**, 38 (2010).
24. Y. Hasegawa, K. Fukumoto, T. Ishima, H. Yamamoto, M. Sano and T. Miyake, *Appl. Catal.: B Environ.*, **89**, 420 (2009).
25. A. Gurbani, J. L. Ayastuy, M. P. González-Marcos and M. A. Gutiérrez-Ortiz, *Int. J. Hydrog. Energy*, **35**, 11582 (2010).
26. K. H. Cho, J.-H. Park and C.-H. Shin, *Clean Tech.*, **16**, 132 (2010).
27. L. Lianjun, Y. Qiang, Z. Jie, W. Haiqin, S. Keqin, L. Bin, Z. Haiyang, G. Fei, D. Lin and X. Chen, *J. Colloid Interf. Sci.*, **195**, 236 (2002).
28. L. Lei, S. Li, W. Haidong, C. Chongqi, S. Yusheng, Z. Yingying, L. Xingyi and Z. Qi, *Int. J. Hydrog. Energy*, **36**, 8839 (2011).